

An estimation of the $^{18}\text{O}/^{16}\text{O}$ ratio of UT/LMS ozone based on artefact CO in air sampled during CARIBIC flights

S. Gromov¹, C. A. M. Brenninkmeijer¹

¹ Max Planck Institute for Chemistry, Mainz, Germany

Correspondence to: S. Gromov (sergey.gromov@mpic.de)

Abstract

An issue of O₃-driven artefact production of CO in the upper troposphere/lowermost stratosphere (UT/LMS) air analysed in the CARIBIC-1 project is being discussed. By confronting the CO mixing and isotope ratios obtained from different analytical instrumentation, we (i) reject natural/artificial sampling and mixing effects as possible culprits of the problem, (ii) ascertain the chemical nature and quantify the strength of the contamination, and (iii) demonstrate successful application of the isotope mass-balance calculations for inferring the isotope composition of the contamination source. The $\delta^{18}\text{O}$ values of the latter indicate the oxygen very likely being inherited from O₃. The $\delta^{13}\text{C}$ values hint at reactions of trace amounts of organics with stratospheric O₃ that could have yielded the artificial CO. While the exact contamination mechanism is not known, it is clear that the issue pertains only to the earlier (first) phase of the CARIBIC project. Finally, estimated UT/LMS ozone $\delta^{18}\text{O}$ values are lower than those observed in the stratosphere within the same temperature range, suggesting that higher pressures (240–270 hPa) imply lower isotope fractionation controlling the local $\delta^{18}\text{O}(\text{O}_3)$ value.

1 Introduction

[1] Accurate determination of the atmospheric carbon monoxide (CO) content based on the collection of air samples depends on the preservation of the mixing ratio of CO inside the receptacle, from the point of sampling to the moment of physicochemical analysis in a laboratory. A well known example in our field of research is the filling of pairs of glass flasks at South Pole

20 Station for analysis at NOAA in Boulder, Colorado, USA (Novelli *et al.*, 1998). There, the du-
21 plicate air sampling allowed for a degree of quality control which in view of the long transit
22 times, especially during polar winter, was a perhaps not perfect, but certainly a practical meas-
23 ure. Here we deal with a different case: Using aircraft-based collection of very large air samples
24 rendered duplicate sampling unpractical, yet analyses could be performed soon after the sam-
25 pling had taken place because of the proximity of the aircraft's landing location to the laborato-
26 ry involved. A presumption of the analytical integrity of the process was that the growth of CO
27 in receptacles is gradual and takes its time. Reminding Thomas Henry Huxley's statement, "The
28 great tragedy of Science – the slaying of a beautiful hypothesis by an ugly fact", it turned out,
29 however, that for air we collected in stainless steel tanks in the upper troposphere/lowermost
30 stratosphere (UT/LMS) higher CO values were measured in the laboratory than measured
31 *in situ* during the collection of these air samples. Moreover, measurement of the stable oxygen
32 isotopic composition of CO from these tanks revealed additional isotopic enrichments in ^{18}O of
33 10‰ or more. It was soon realised that this phenomenon was due to the formation of CO in
34 these tanks and/or possibly in the sampling system and inlet tubing used, by reactions involving
35 ozone (Brenninkmeijer *et al.*, 1999).

36 [2] Unexpectedly high $^{18}\text{O}/^{16}\text{O}$ ratios in stratospheric ozone (O_3) were discovered by Konrad
37 Mauersberger using a balloon-borne mass spectrometer (Mauersberger, 1981), which has trig-
38 gered a series of theoretical and experimental studies on atmospheric O_3 heavy isotope enrich-
39 ments (see, *e.g.*, Schinke *et al.* (2006) for a review). In view of the advances in theoretical and
40 laboratory studies on the isotopic composition of O_3 atmospheric measurements are welcome,
41 they do however form a challenge. In the stratosphere O_3 number concentrations are high, but
42 the remoteness of the sampling domain is a problem. In the troposphere, low O_3 number densi-
43 ties are the main obstacle, as indicated by few experiments performed to date
44 (Krankowsky *et al.*, 1995; Johnston and Thiemens, 1997; Vicars and Savarino, 2014). Never-
45 theless, recent analytical improvements, namely the use of an indirect method of reacting at-
46 mospheric O_3 with a substrate that can be analysed for the isotopic composition of the
47 O_3 -derived oxygen (Vicars *et al.*, 2012), has greatly improved our ability to obtain information
48 on the O_3 isotopic composition.

49 [3] Although the increase of CO concentrations in air stored in vessels is a well recognised
50 problem, to our knowledge a specific O_3 -related process has not been reported yet. Here we dis-
51 cuss this phenomenon and turn its disadvantage into an advantage, namely that of obtaining an
52 estimate of the oxygen isotopic composition of O_3 in the UT/LMS, an atmospheric domain not

53 yet covered by specific measurements. The air samples we examine in this study were collected
54 onboard a passenger aircraft carrying an airfreight container with analytical and air/aerosol
55 sampling equipment on long distance flights from Germany to South India and the Caribbean
56 within the framework of the CARIBIC project (Civil Aircraft for the Regular Investigation of
57 the atmosphere Based on an Instrument Container, <http://www.caribic-atmospheric.com>).

58 **2 Experimental and results**

2.1 Whole air sampling

59 [4] CARIBIC-1 (Phase #1, abbreviated hereafter “C1”) was operational from November 1998
60 until April 2002 using a *Boeing 767-300 ER* operated by LTU International Airlines
61 (Brenninkmeijer *et al.*, 1999). Using a whole air sample (WAS) collection system, twelve air
62 samples were collected per flight (of 8–10 hours duration at cruise altitudes of 10–12 km) in
63 stainless steel tanks for subsequent laboratory analysis of the mixing ratios (*i.e.* mole fractions)
64 of various trace gases, including ^{14}CO . Large air samples were required in view of the ultra-low
65 number density of this mainly cosmogenic tracer (10–100 molecules cm^{-3} standard temperature
66 and pressure (STP), about 0.4–4 amol/mol). Hereinafter STP denotes dry air at 273.15 K,
67 101325 Pa. Each C1 WAS sample (holding 350 litres of air STP) was collected over 15–20 min
68 intervals representing the number density-weighted average of the compositions encountered
69 along flight segments of about 250 km. The overall uncertainty of the measured WAS CO is
70 less than $\pm 1\%$ for the mixing ratio and $\pm 0.1\text{‰}/\pm 0.2\text{‰}$ for $\delta^{13}\text{C}(\text{CO})/\delta^{18}\text{O}(\text{CO})$, respectively
71 (Brenninkmeijer, 1993; Brenninkmeijer *et al.*, 2001). Isotope compositions are reported
72 throughout this manuscript using the so-called delta value $\delta = (R/R_{\text{st}} - 1)$ relating the ratio R of
73 rare (^{13}C , ^{18}O or ^{17}O) over abundant isotopes of interest to the standard ratio R_{st} . These are Vi-
74 enna Standard Mean Ocean Water (VSMOW) for $^{18}\text{O}/^{16}\text{O}$ (Gonfiantini, 1978; Coplen, 1994)
75 and $^{17}\text{O}/^{16}\text{O}$ (Assonov and Brenninkmeijer, 2003), and Vienna Pee Dee Belemnite (VPDB) for
76 $^{13}\text{C}/^{12}\text{C}$ (Craig, 1957), respectively. As we mention above, the oxygen isotope composition of
77 the CO present in these WAS samples was corrupted, in particular when O_3 levels were as high
78 as 100–600 nmol/mol.

79 [5] CARIBIC-2 (Phase #2, referred to as “C2”) started operation in December 2004 with a
80 Lufthansa *Airbus A340-600* fitted with a new inlet system and air sampling lines, including per-
81 fluoroalkoxy alkane (PFA) lined tubing for trace gas intake (Brenninkmeijer *et al.*, 2007). No
82 flask CO mixing/isotope ratio measurements are performed in C2.

2.2 On-line instrumentation

83 [6] In addition to the WAS collection systems, both C1 and C2 measurement setups include dif-
84 ferent instrumentation for on-line detection of [CO] and [O₃] (hereinafter the squared brackets
85 [] denote the mixing ratio of the respective species). *In situ* CO analysis in C1 is done using a
86 gas chromatography (GC)-reducing gas analyser which provides measurements every 130 s
87 with an uncertainty of ± 3 nmol/mol (Zahn *et al.*, 2000). In C2, a vacuum ultraviolet fluores-
88 cence (VUV) instrument with lower measurement uncertainty and higher temporal resolution of
89 ± 2 nmol/mol in 2 s (Scharffe *et al.*, 2012) is employed. Furthermore, the detection frequency
90 for O₃ mixing ratios has also increased, *viz.*, from 0.06 Hz in C1 to 5 Hz in C2
91 (Zahn *et al.*, 2002; Zahn *et al.*, 2012).

2.3 Results

92 [7] When comparing the CO mixing ratios in relation to those of O₃ for C1 and C2, differences
93 are apparent in the LMS, where C2 [CO] values are systematically lower. This is illustrated in
94 Fig. 1 (a) which presents the LMS CO-O₃ distribution of the C2 *in situ* measurements overlaid
95 with the C1 *in situ* and WAS data. The entire C1 CO/O₃ dataset is presented in Fig. 2. For the
96 *in situ* CO datasets we calculated the statistics (Fig. 1 (b)) of the samples with respective O₃
97 mixing ratios clustered in 20 nmol/mol bins, *i.e.* the median and spread of [CO] as a function of
98 [O₃] analysed. The interquartile range, IQR, is used in the current analysis as a robust measure
99 of the data spread instead of the standard deviation. The LMS data exhibit large [CO] variations
100 for [O₃] between 300 and 400 nmol/mol, which primarily reflect pronounced seasonal varia-
101 tions in the NH tropospheric CO mixing ratio. With increasing [O₃], [CO] decreases to typical
102 stratospheric values, and its spread reduces to mere 3.5 nmol/mol and less, as [O₃] surpasses
103 500 nmol/mol. Despite the comparable spread in C1 and C2 [CO], from 400 nmol/mol of [O₃]
104 onwards the C1 CO mixing ratios start to level off, with no samples below 35 nmol/mol having
105 been detected, whereas the C2 levels continuously decline. By the 570–590 nmol/mol O₃ bin,
106 C1 [CO] of $39.7^{+0.3}_{-0.3}$ nmol/mol contains some extra 14 nmol/mol compared to $25.6^{+1.7}_{-1.7}$ nmol/mol
107 typical for C2 values. Overall, at [O₃] above 400 nmol/mol the conspicuously high [CO] is
108 marked in about 200 *in situ* C1 samples, of which 158 and 69 emerge as statistically significant
109 mild and extreme outliers, respectively, when compared against the number of C2 samples
110 ($n > 3 \cdot 10^5$). The conventions here follow Natrella (2003), *i.e.* ± 1.5 and ± 3 IQR ranges define the
111 inner and outer statistical fences (ranges outside which the data points are considered mild and
112 extreme outliers) of the C2 [CO] distribution in every O₃ bin, respectively. The statistics include

113 the samples in bins with average $[O_3]$ of 420–620 nmol/mol. None of C1 CO at $[O_3]$ above
114 560 nmol/mol agrees with the C2 observations. Because the CO- O_3 distribution cannot have
115 changed over the period in question, we find that an apparent relative excess CO of up to 55%
116 justifies and investigation into sampling artefacts and calibration issues.

117 [8] Unnatural elevations in $\delta^{18}O(CO)$ from WAS measurements are also evident, as shown in
118 Figs. 3 and 4. The large $\delta^{18}O(CO)$ elevations that reach beyond +16‰ are found to be propor-
119 tional to the concomitant O_3 mixing ratios (denoted with colour) and are more prominent at
120 lower $[CO]$. Lower $\delta^{18}O(CO)$ values, however, are expected based on our knowledge of UT/
121 LMS CO sources (plus their isotope signatures) and available *in situ* observations (Fig. 3,
122 shown with triangles), as elucidated by Brenninkmeijer *et al.* (1996) (hereafter denoted as
123 “B96”). That is, the greater the proportion of stratospheric CO, the greater its fraction stemming
124 from methane oxidation with a characteristic $\delta^{18}O$ of 0‰ or lower (Brenninkmeijer and Röck-
125 mann, 1997). This occurs because the CO sink at ruling UT/LMS temperatures proceeds more
126 readily than its production, as the reaction of hydroxyl radical (OH) with CO, being primarily
127 pressure-dependent, is faster than the temperature-sensitive reaction of OH with CH_4 . Further-
128 more, as the lifetime of CO quickly decreases with altitude, transport-mixing effects take the
129 lead in determining the vertical distributions of $[CO]$ and $\delta^{18}O(CO)$ above the tropopause,
130 hence their mutual relationship. This is seen from the B96 data at $[CO]$ below 50 nmol/mol that
131 line-up in a near linear relationship towards the end-members with lowest $^{18}O/^{16}O$ ratios. These
132 result from the largest share of the ^{18}O -depleted photochemical component and extra depletion
133 caused by the preferential removal of $C^{18}O$ in reaction with OH (fractionation about +11‰ at
134 pressures below 300 hPa, Stevens *et al.*, 1980; Röckmann *et al.*, 1998b).

135 [9] We are confident that the enhancements of C1 $C^{18}O$ originate from O_3 , whose large enrich-
136 ment in ^{18}O (above +60‰ in $\delta^{18}O$, Brenninkmeijer *et al.*, 2003) is typical and found transferred
137 to other atmospheric compounds (see Savarino and Morin (2012) for a review). In Fig. 3 it is al-
138 so notable that not only the LMS compositions are affected but elevations of (3–10)‰ from the
139 bulk $\delta^{18}O(CO)$ values are present in more tropospheric samples with $[CO]$ of up to
140 100 nmol/mol. These result from the dilution of the least affected CO-rich tropospheric air by
141 CO-poor, however substantially contaminated, stratospheric air, sampled into the same WAS
142 tank. Such sampling-induced mixing renders an unambiguous determination of the artefact
143 source’ isotope signature rather difficult, because neither mixing nor isotope ratios of the ad-
144 mixed air portions are known sufficiently well (see below).

145 [10] Differences between the WAS and *in situ* measured [CO] – a possible indication that the
146 $\delta^{18}\text{O}(\text{CO})$ contamination pertains specifically to the WAS data – average at $\bar{\Delta}(\text{WAS}-\textit{in situ}) =$
147 (5.3 ± 0.2) nmol/mol (± 1 standard deviation of the mean, $n = 408$) and happen to be random with
148 respect to any operational parameter or measured characteristic in C1, *i.e.* irrespective of CO or
149 O_3 abundances. The above mentioned discrepancy remained after several calibrations between
150 the two systems had been performed, and likely results from the differences in the detection
151 methods, drifts of the calibration standards used (see details in Brenninkmeijer *et al.*, 2001) and
152 a short-term production of CO in the stainless steel tanks during sampling. The large spread of
153 $\Delta(\text{WAS}-\textit{in situ})$ of ± 3.5 nmol/mol ($\pm 1\sigma$ of the population) ensues from the fact that the *in situ*
154 sampled air corresponds to (2–4)% of the concomitantly sampled WAS volume, as typically
155 6–7 *in situ* collections of 5 s were made throughout one tank collection of 17–21 min. The in-
156 tegrity of the WAS CO is further affirmed by the unsystematic distribution of the artefact com-
157 positions among tanks (in contrast to that for $\delta^{18}\text{O}(\text{CO}_2)$ in C1 discussed by As-
158 sonov *et al.*, 2009). Overall, the WAS and *in situ* measured CO mixing ratios correlate extreme-
159 ly well (adj. $R^2 = 0.972$, slope of 0.992 ± 0.008 ($\pm 1\sigma$), $n = 408$). However, both anomalies in
160 [CO] and $\delta^{18}\text{O}(\text{CO})$ manifest clear but complex influences of the concomitant [O_3]. That is, the
161 C1 *in situ* and WAS [CO] and $\delta^{18}\text{O}(\text{CO})$ data very likely evidence artefacts pertaining to the
162 same O_3 -driven effect. Below we discuss and quantify these influences.

163 3 Discussion

164 [11] Three factors may lead to the (artefact) distributions seen for C1 *in situ* [CO] at LMS O_3
165 mixing ratios, namely:

166 [12] (i) Strong (linear) natural mixing, such as enhanced stratosphere-troposphere exchange
167 (STE), when a [CO] outside the statistically expected range results from the integration of air
168 having dissimilar ratios of the tracers' mixing ratios, *viz.* [O_3]:[CO]. For example, mixing of
169 two air parcels in a 16%:84% proportion (by moles of air) with typical [O_3]:[CO] of 700:24
170 (stratospheric) and 60:125 (tropospheric), respectively, yields an integrated composition with
171 [O_3]:[CO] of 598:40 which indeed corresponds to C1 data (this case is exemplified by the mix-
172 ing curve in Fig. 1). Nonetheless, occurrences of rather high stratospheric CO mixing ratios (in
173 our case, 40 nmol/mol at the concomitant [O_3] of 500–600 nmol/mol compared to the typical
174 24–26 nmol/mol) are rare. For instance, a deep STE similar to that described by
175 Pan *et al.* (2004) was observed by C2 only once (*cf.* the outliers at [O_3] of 500 nmol/mol in
176 Fig. 1), whereas the C1 outliers were exclusively registered in some 12 flights during

177 1997–2001. No relation between these outliers and the large-scale [CO] perturbation due to ex-
178 tensive biomass burning in 1997/1998 (Novelli *et al.*, 2003) is established, otherwise elevated
179 CO mixing ratios should manifest themselves at lower [O₃] as well. Other tracers detected in
180 CARIBIC provide supporting evidence against such strongly STE-mixed air having been cap-
181 tured by C1. That is, the binned distributions for water vapour and de-trended N₂O mixing rati-
182 os (not shown here) are similar for C1 and C2. Whereas the small relative variations in atmos-
183 pheric [N₂O] merely confirm matching [O₃] distributions in CARIBIC, the stratospheric [H₂O]
184 distributions witness no [O₃]:[H₂O] values corresponding to those of the C1 outliers, suggesting
185 the latter being unnaturally low.

186 [13] (ii) Mixing effects can also occur artificially, originating from sampling peculiarities or data
187 processing. Since the CARIBIC platform is not stationary, about 5 s long sampling of an *in situ*
188 air probe in C1 implies integration of the air compositions encountered along some hundred me-
189 tres, owing to the high aircraft speed. This distance may cover a transect between tropospheric
190 and stratospheric filaments of different compositions. The effect of such ‘translational mixing’
191 can be simulated by averaging the sampling data with higher temporal frequency over longer
192 time intervals. In this respect, the substantially more frequent CO data in C2 (sampling interval
193 <1 s) were artificially averaged over a set of increasing intervals to reckon whether the long
194 sampling period in C1 could be the culprit for skewing its CO–O₃ distribution. As a result, the
195 original C2 data and their averages (equivalent to the C1 CO sample injection time) differ neg-
196 ligibly, as do the respective [O₃]:[CO] values. Our simulations of the ‘translational mixing’ ef-
197 fects confirm that the actual C2 CO–O₃ distribution in the region of interest ([O₃] of
198 540–620 nmol/mol) remains insensitive to averaging intervals of up to 300 s. Furthermore, a
199 very strong artificial mixing with an averaging interval of at least 1200 s (comparable to C1
200 WAS sampling time) is required to yield the averages from the C2 data with [O₃]:[CO] charac-
201 teristic for the C1 outliers.

202 [14] (iii) In view of the above, it is unlikely that any natural or artificial mixing processes are in-
203 volved in the stratospheric [CO] discrepancies seen in C1. We therefore conclude that the sam-
204 ple contamination in C1 occurred prior to the probed air reaching the analytical instrumentation
205 and WAS sampling tanks in the container, since clearly elevated stratospheric CO mixing ratios
206 are common to WAS and *in situ* data. Two more indications, *viz.* growing [CO] discrepancy
207 with increasing O₃ abundance, and the strong concomitant signal in δ¹⁸O(CO), suggest that O₃-
208 mediated production of CO took place. Further, by confronting the C1 and C2 [CO] measure-

209 ments in a regression analysis (detailed in Appendix A), we quantify the artefact component
 210 CO_c being chiefly a function of O_3 mixing ratio as

$$[\text{CO}_c] = b \cdot [\text{O}_3]^2, \quad b = (5.19 \pm 0.12) \cdot 10^{-5} \text{ [mol/nmol]}, \quad (1)$$

211 which is equivalent to 8–18 nmol/mol throughout the respective $[\text{O}_3]$ range of
 212 400–620 nmol/mol (see Fig. 1 (d)). Subtracting this artefact signal yields the corrected *in situ*
 213 C1 CO – O_3 distribution conforming to that of C2 (*cf.* red symbols in Fig. 1 (a)).

214 [15] Importantly, since we can quantify the contamination strength using only the O_3 mixing ra-
 215 tio, the continuous *in situ* C1 $[\text{O}_3]$ data allow estimating the integral artefact CO component in
 216 each WAS sample and, if the isotope ratio of contaminating O_3 is known, to derive the initial
 217 $\delta^{18}\text{O}(\text{CO})$. The latter, as it was mentioned above, is subject to strong sample-mixing effects,
 218 which is witnessed by $\delta^{18}\text{O}(\text{CO})$ outliers even at relatively high $[\text{CO}]$ up to 100 nmol/mol. Ac-
 219 counting for such cases is, however, problematic since it is necessary to distinguish the propor-
 220 tions of the least modified (tropospheric) and significantly affected (stratospheric) components
 221 in the resultant WAS sample mix. Since this information is not available, we applied an *ad hoc*
 222 correction approach, as described in the following. This approach is capable of determining the
 223 contamination source (*i.e.*, O_3) isotope signature as well.

3.1 Contamination isotope signatures

224 [16] We use the differential mixing model (MM, originally known as the “Keeling-plot”) in
 225 combination with the parameterisation of the artefact CO component (Eq. (1)) to derive the iso-
 226 topic composition of the latter. This approach makes no assumptions on the isotope signatures
 227 of CO in the air portions mixed in a given WAS tank. The MM parameterises the admixing of
 228 the portion of artefact CO to the WAS sample with the “true” initial composition, as formulated
 229 below:

$$[\text{CO}] = [\text{CO}_t] + [\text{CO}_c], \quad (2)$$

$$\delta(\text{CO})[\text{CO}] = \delta(\text{CO}_t)[\text{CO}_t] + \delta(\text{CO}_c)[\text{CO}_c], \quad (3)$$

230 where indices *c* and *t* distinguish the components pertaining to the estimated contamination and
 231 “true” composition sought (*i.e.*, $[\text{CO}_t]$ and $\delta(\text{CO}_t)$), respectively. Here the contamination
 232 strength $[\text{CO}_c]$ is derived by integrating Eq. (1) using the *in situ* C1 $[\text{O}_3]$ data for each WAS
 233 sample. By rewriting the above equation with respect to the isotope signature of the analysed
 234 CO , one obtains:

$$\delta(\text{CO}) = \delta(\text{CO}_c) + (\delta(\text{CO}_t) - \delta(\text{CO}_c)) [\text{CO}_t]/[\text{CO}], \quad (4)$$

235 which signifies that linear regression of $\delta(\text{CO})$ as a function of the reciprocal of $[\text{CO}]$ yields the
236 estimated contamination signature $\delta(\text{CO}_c)$ at $([\text{CO}])^{-1} \rightarrow 0$ when invariable "true" compositions
237 ($[\text{CO}_i]$, $\delta(\text{CO}_i)$) are taken (the Keeling plot detailing these calculations is shown in Fig. 5). We
238 therefore apply the MM described by Eq. (4) to the subsets of samples picked according to the
239 same reckoned $[\text{CO}_i]$ (within a ± 2 nmol/mol window, $n > 7$). Such selection, however, may be
240 insufficient: Due to the strong sampling effects in the WAS samples (see previous Section), it is
241 possible to encounter samples that integrate different air masses to the same $[\text{CO}_i]$ but rather
242 different average $\delta(\text{CO}_i)$. The solution in this case is to refer to the goodness of the MM regres-
243 sion fit, because the R^2 intrinsically measures the linearity of the regressed data, *i.e.* closeness of
244 the "true" values in a regarded subset of samples, irrespective of underlying reasons for that.

245 [17] Higher R^2 values thus imply higher consistency of the estimate, as demonstrated in Fig. 6
246 showing the calculated $\delta(\text{CO}_c)$ for $[\text{CO}_i]$ below 80 nmol/mol as a function of the regression R^2 .
247 The latter decreases with greater $[\text{CO}_i]$ (*i.e.*, larger sample subset size, since tropospheric air is
248 more often encountered) and, correspondingly, larger variations in $\delta(\text{CO}_i)$. Ultimately, at lower
249 R^2 the inferred $\delta^{18}\text{O}(\text{CO}_c)$ converge to values slightly above zero expected for uncorrelated data,
250 *i.e.* C1 $\delta^{18}\text{O}(\text{CO})$ tropospheric average. A similar relationship is seen for the $\delta^{13}\text{C}(\text{CO}_c)$ values
251 (they converge around -28‰), however, there are no consistent estimates found (R^2 is generally
252 below 0.4). Since such is not the case for $\delta^{18}\text{O}$, the MM is not sufficiently sensitive to the
253 changes caused by the contamination, which implies that the artefact CO $\delta^{13}\text{C}$ should be within
254 the range of the "true" $\delta^{13}\text{C}(\text{CO})$ values. Interestingly, the MM is rather responsive to the grow-
255 ing fraction of the CH_4 -derived component in CO with increasing $[\text{O}_3]$, as the $\delta^{13}\text{C}(\text{CO}_c)$ value
256 of $-(47.2 \pm 5.8)\text{‰}$ inferred at R^2 above 0.4 is characteristic for the $\delta^{13}\text{C}$ of methane in the UT/
257 LMS. It is important to note that we have accounted for the biases in the analysed C1 WAS
258 $\delta^{13}\text{C}(\text{CO})$ expected from the mass-independent isotope composition of O_3 (see details in Ap-
259 pendix B).

260 [18] We derive the "best-guess" estimate of the admixed CO ^{18}O signature at $\delta^{18}\text{O}(\text{CO}_c) =$
261 $+(92.0 \pm 8.3)\text{‰}$, which agrees with the other MM results obtained at R^2 above 0.75. Taking the
262 same subsets of samples, the concomitant ^{13}C signature matches $\delta^{13}\text{C}(\text{CO}_c) = -(23.3 \pm 8.6)\text{‰}$,
263 indeed at the upper end of the expected LMS $\delta^{13}\text{C}(\text{CO})$ variations of $-(25-31)\text{‰}$. Because of
264 that, the MM is likely insensitive to the changes in $\delta^{13}\text{C}(\text{CO})$ caused by the contamination (the
265 corresponding R^2 values are below 0.1). Upon the correction using the inferred $\delta^{18}\text{O}(\text{CO}_c)$ val-
266 ue, the C1 WAS $\delta^{18}\text{O}(\text{CO})$ data agree with B96 (shown with red symbols in Fig. 3). That is,
267 variations in the observed C^{18}O are driven by (i) the seasonal/regional changes in the composi-

268 tion of tropospheric air and by (ii) the degree of mixing or replacement of the latter with the
269 stratospheric component that is less variable in ^{18}O . This is seen as stretching of the scattered
270 tropospheric values ($[\text{CO}]$ above 60 nmol/mol) towards $\delta^{18}\text{O}(\text{CO})$ of around -10% at $[\text{CO}]$ of
271 25 nmol/mol, respectively. The corrected C1 $\delta^{13}\text{C}(\text{CO})$ data (shown in Fig. 7) are found to be in
272 a $\pm 1\%$ agreement with the observations by B96, except for several deep stratospheric samples
273 ($[\text{CO}]$ below 40 nmol/mol). The latter were encountered during “ozone hole” conditions and
274 carried extremely low $\delta^{13}\text{C}(\text{CO})$ values, which was attributed to the reaction of methane with
275 available free Cl radicals (Brenninkmeijer *et al.*, 1996).

3.2 Estimate of $\delta^{18}\text{O}(\text{O}_3)$

276 [19] The contamination ^{18}O signature inferred here ($\delta^{18}\text{O}(\text{CO}_c) = +(92.0 \pm 8.3)\%$) likely pertains
277 to O_3 and is comparable to $\delta^{18}\text{O}(\text{O}_3)$ values measured in the stratosphere at temperatures about
278 30 K lower than those encountered in the UT/LMS by C1 (see Table 1 for comparison). If no
279 other factors are involved (see below), this discrepancy in $\delta^{18}\text{O}(\text{O}_3)$ should be attributed to the
280 local conditions, *i.e.* the higher pressures (typically 240–270 hPa for C1 cruising altitudes) at
281 which O_3 was formed. Indeed, the molecular lifetime (the period through which the species’
282 isotope reservoir becomes entirely renewed, as opposed to the “bulk” lifetime) of O_3 encoun-
283 tered along the C1 flight routes is estimated on the order of minutes to hours at daylight
284 (H. Riede, Max Planck Institute for Chemistry, 2010), thus the isotope composition of the pho-
285 tochemically regenerated O_3 resets quickly according to the local conditions. Virtual absence of
286 sinks, in turn, leads to “freezing” of the $\delta^{18}\text{O}(\text{O}_3)$ value during night in the UT/LMS. Verifying
287 the current $\delta^{18}\text{O}(\text{O}_3)$ estimate against the kinetic data, in contrast to the stratospheric cases, is
288 problematic. The laboratory studies on O_3 formation to date have scrutinised the concomitant
289 kinetic isotope effects (KIEs) as a function of temperature at only low pressures (67 mbar); the
290 attenuation of the KIEs with increasing pressure was studied only at room temperatures (see
291 Table 1, also Brenninkmeijer *et al.* (2003) for references). A rather crude attempt may be under-
292 taken by assuming that the formation KIEs become attenuated at higher pressures in a similar
293 (proportional) fashion to that measured at 320 K, however applied to the nominal low-pressure
294 values reckoned at (220–230) K. A decrease in $\delta^{18}\text{O}(\text{O}_3)$ of about (6–8)% is expected from
295 such calculation (*cf.* last row in Table 1), yet accounting for a mere one-half of the (13–15)%
296 discrepancy between the stratospheric $\delta^{18}\text{O}(\text{O}_3)$ values and $\delta^{18}\text{O}(\text{CO}_c)$.

297 [20] Lower $\delta^{18}\text{O}(\text{CO}_c)$ values could result from possible isotope fractionation accompanying the
298 production of the artefact CO. Although not quantifiable here, oxygen KIEs in the $\text{O}_3 \rightarrow \text{CO}$

299 conversion chain cannot be ruled out, recalling that the intermediate reaction steps are not iden-
300 tifiable and the artefact CO represents at most 4% of all O₃ molecules. Furthermore, the yield
301 λ_{O_3} of CO from O₃ may be lower than unity (see details in Appendix A). On the other hand, the
302 inference that the contamination strength primarily depends on [O₃] indicates that the kinetic
303 fractionation may have greater effect on the carbon isotope ratios of the artefact CO produced
304 (the $\delta^{13}C(CO_c)$ values) in contrast to the oxygen ones. That is because all reactive oxygen avail-
305 able from O₃ becomes converted to CO, whilst the concomitant carbon atoms are drawn from a
306 virtually unlimited pool whose apparent isotope composition is altered by the magnitude of the
307 ¹³C KIEs.

308 [21] Besides KIEs, selectivity in the transfer of O atoms from O₃ to CO affects the resulting
309 $\delta^{18}O(CO_c)$ value. The terminal O atoms in O₃ are enriched with respect to the molecular (bulk)
310 O₃ composition when the latter is above +70‰ in $\delta^{18}O$ (Janssen, 2005; Bhattachar-
311 ya *et al.*, 2008), therefore an incorporation of only central O atoms into the artefact CO mole-
312 cules should result in a reduced apparent $\delta^{18}O(CO_c)$ value. Such exclusive selection is, howev-
313 er, less likely from the kinetic standpoint and was not observed in available laboratory studies
314 (see Savarino *et al.* (2008) for a review). For instance, Röckmann *et al.* (1998a) established the
315 evidence of direct O transfer from O₃ to the CO produced in alkene ozonolysis. A reanalysis of
316 their results (in light of findings of Bhattacharya *et al.* (2008)) suggests that usually the terminal
317 atoms of the O₃ molecule become transferred (their ratio over the central ones changes from the
318 bulk 2:1 to 1:0 for various species). Considering the alternatives of the O transfer in our case
319 (listed additionally in Table 1), the equiprobable incorporation of the terminal and central O₃
320 atoms into CO should result in the $\delta^{18}O(O_3)$ value in agreement with the “crude” estimate based
321 on laboratory data given above.

322 [22] Furthermore, the conditions that supported the reaction of O₃ (or its derivatives) followed by
323 the production of CO are vague. A few hypotheses ought to be scrutinised here. First, a fast
324 O₃ → CO conversion must have occurred, owing to short (*i.e.*, fraction of a second) exposure
325 time of the probed air to the contamination. Accounting for the typical C1 air sampling condi-
326 tions (these are: sampled air pressure of 240–270 hPa and temperature of 220–235 K outboard
327 to 275–300 K inboard, sampling rate of $12.85 \cdot 10^{-3}$ mol s⁻¹ corresponding to 350 L STP sam-
328 pled in 1200 s, inlet/tubing volume gauged to yield exposure times of 0.01 to 0.1 s due to varia-
329 ble air intake rate, [O₃] of 600 nmol/mol), the overall reaction rate coefficient (k_c in Eq. (A3)
330 from Appendix A) must be on the order of $(6 \cdot 10^{-15}/\tau_c)$ molecules⁻¹ cm³, where τ_c is the exposure
331 time. Assuming the case of a gas-phase CO production from a recombining O₃ derivative and

332 an unknown carbonaceous compound X, the reaction rate coefficient for the latter (k in Eq. (A2)
333 in Appendix A) must be unrealistically high, at least $6 \cdot 10^{-10} \text{ molec}^{-1} \text{ cm}^3 \text{ s}^{-1}$ over $\tau_c = 1/100 \text{ s}$.
334 This number decreases proportionally with growing τ_c and $[X]$, if we take less strict exposure
335 conditions. Nonetheless, in order to provide the amounts of artefact CO we detect, a minimum
336 mixing ratio of 20 nmol/mol (or up to 4 μg of C per flight) of X is required, which is not availa-
337 ble in the UT/LMS from the species readily undergoing ozonolysis, *e.g.* alkenes.

338 [23] Second, a more complex heterogeneous chemistry on the inner surface of the inlet or sup-
339 plying tubing may be involved. Such can be the tracers' surface adsorption, (catalytic) decom-
340 position of O_3 and its reaction with organics or with surface carbon that also may lead to the
341 production of CO (Oyama, 2000). Evidence exists for the dissociative adsorption of O_3 on the
342 surfaces with subsequent production of the reactive atomic oxygen species (see, *e.g.*,
343 Li *et al.*, 1998, also Oyama, 2000). It is probable that sufficient amounts of organics have re-
344 mained on the walls of the sampling line exposed to highly polluted tropospheric air, to be later
345 broken down by the products of the heterogeneous decomposition of the ample stratospheric O_3 .
346 Unfortunately, the scope for a detailed quantification of intricate surface effects in the C1 CO
347 contamination problem is very limited.

348 **4 Conclusions**

349 [24] Recapitulating, the *in situ* measurements of CO and O_3 allowed us to unambiguously quanti-
350 fy the artefact CO production from O_3 likely in the sample line of the CARIBIC-1 instrumenta-
351 tion. Strong evidence to that is provided by the isotope CO measurements. We demonstrate the
352 ability of the simple mixing model ("Keeling-plot" approach) to single out the contamination
353 isotope signatures even in the case of a large sampling-induced mixing of the air with very dif-
354 ferent compositions. Obtained as a collateral result, the estimate of the $\delta^{18}\text{O}(\text{O}_3)$ in the UT/LMS
355 appears adequate, calling, however, for additional laboratory data (*e.g.*, the temperature-driven
356 variations of the O_3 formation KIE at pressures above 100 hPa) for a more unambiguous verifi-
357 cation.

358 **Appendix A. Contamination assessment**

359 [25] We quantify the C1 CO contamination strength (denoted $[\text{CO}_c]$, obtained by discriminating
360 the C1 outliers from respective C2 data) in a sequence of regression analyses. We foremost as-
361 certain that no other species or operational parameter (*e.g.* temperature, pressure, flight dura-

362 tion, season, latitude, time of day, *etc.*) measured in C1 appear to determine (*e.g.*, systematically
 363 correlate with) $[\text{CO}_c]$, except that for $[\text{O}_3]$. We hypothesise therefore that a production of arte-
 364 fact CO molecules was initiated by O_3 (via either its decomposition or a reaction with an un-
 365 known educt) and proceeded with incorporation of carbon (donated by some carbonaceous spe-
 366 cies X) and oxygen (donated by O_3 or its derivatives) atoms into final CO. Despite that neither
 367 the actual reaction chain nor its intermediates are known, it is possible to describe the artefact
 368 component CO_c produced (hereinafter curly brackets $\{\}$ denote number densities) as

$$\{\text{CO}_c\} = \lambda_{\text{O}_3} \nu \tau_c, \quad (\text{A1})$$

369 where the yield λ_{O_3} , a diagnostic quantity, relates the amount of artefact CO molecules produced
 370 to the total number of O_3 molecules consumed in the system, τ_c denotes the reaction time (peri-
 371 od throughout which sampled air is exposed to contamination), and ν stands for the overall rate
 372 of the reaction chain. The latter, being regarded macroscopically (empirically), is parameterised
 373 to account for the order of reaction chain rate with respect to hypothesised reactants
 374 (McNaught and Wilkinson, 1997) as

$$\nu = k \{\text{X}\}^K \{\text{O}_3\}^\kappa, \quad (\text{A2})$$

375 where κ and K are the partial orders with respect to X and O_3 number densities, respectively,
 376 and k is the rate coefficient. Here it is implied that changes to $\{\text{X}\}$ and $\{\text{O}_3\}$ are negligible
 377 throughout the exposure time τ_c (typically < 0.1 s for C1 sample line). As stated above, we find
 378 that variations in $\{\text{CO}_c\}$ correlate exclusively with variations in $\{\text{O}_3\}$, hence Eq. (A2) can be
 379 reduced by assuming constancy of $\{\text{X}\}$ and K to:

$$\nu_c = k_c \{\text{O}_3\}^\kappa. \quad (\text{A3})$$

380 Here, $k_c = k \{\text{X}\}^K$ (often referred to as pseudo-first-order or “observed” rate coefficient) quanti-
 381 fies the rate of reaction chain exclusively propelled by O_3 . Finally, using Eqs. (A1) and (A3),
 382 the artefact $\{\text{CO}_c\}$ component is expressed as

$$\{\text{CO}_c\} = b \cdot \{\text{O}_3\}^\kappa, \quad b = \lambda_{\text{O}_3} k_c \tau_c \quad (\text{A4})$$

383 where the constant proportionality factor b integrates the influence of the unknown (and as we
 384 explicate below, likely invariable) $\{\text{X}\}$, k , K and τ_c .

385 [26] Eq. (A4) defines the regression expression using which we attempt to fit the values of
 386 $\{\text{CO}_c\}$ as a function of κ , $\{\text{O}_3\}$ and b . In the first regression iteration we keep both κ and b as
 387 free parameters, which provides best approximation at $\kappa = 2.06 \pm 0.38$, suggesting reactions of
 388 two O_3 molecules in case elementary reactions constitute the reaction mechanism, or two ele-
 389 mentary steps involving O_3 or its derivatives in case a stepwise reaction is involved

390 (McNaught and Wilkinson, 1997). In a subsequent regression iteration we set $\kappa = 2$, which
391 yields better (as opposed to the first iteration) estimate of b of $(5.19 \pm 0.12) \cdot 10^{-5}$ mol/nmol ($\pm 1\sigma$,
392 adj. $R^2 = 0.83$, red. $\chi^2 = 4.0$; here the value of b in mole fraction units is derived using the air
393 density at C1 sampling conditions for relating fitted $[\text{CO}_c]$ and observed $[\text{O}_3]^2$). At last, we as-
394 certain that the best regression results are obtained particularly at $\kappa = 2$, as indicated by the re-
395 gression statistic (R^2 and χ^2) that asymptotically improves when a set of regressions with neigh-
396 bouring (*i.e.* below and above 2) integer values of κ is compared. The low uncertainty (within
397 $\pm 3\%$) associated with the estimate of b confirms an exclusive dependence of the contamination
398 source on the O_3 mixing ratio, as well as much similar reaction times τ_c . The regressed value of
399 $[\text{CO}_c]$ as a function of $[\text{O}_3]$ is presented in Fig. 1 (d) (solid line). It is possible to constrain the
400 overall yield λ_{O_3} of CO molecules in the artefact source chain to be between 0.5 and 1, compar-
401 ing the magnitude of $[\text{CO}_c]$ to the discrepancy between the $[\text{O}_3]$ measured in C1 and C2
402 (± 20 nmol/mol, taken equal to the $[\text{O}_3]$ bin size owing to the $\text{N}_2\text{O}-\text{O}_3$ and $\text{H}_2\text{O}-\text{O}_3$ distributions
403 matching well between the datasets). Lower λ_{O_3} values, otherwise, should have resulted in a no-
404 ticeable (*i.e.*, greater than 20 nmol/mol) decrease in the C1 O_3 mixing ratios with respect to the
405 C2 levels.

406 **Appendix B. Corrections to measured $\delta^{13}\text{C}(\text{CO})$ values due to the oxygen**

407 **MIF**

408 [27] Atmospheric O_3 carries an anomalous isotope composition (or mass-independent fractiona-
409 tion, MIF) with a substantially higher relative enrichment in ^{17}O over that in ^{18}O (above +25‰
410 in $\Delta^{17}\text{O} = (\delta^{17}\text{O}+1)/(\delta^{18}\text{O}+1)^\beta - 1$, $\beta = 0.528$) when compared to the majority of terrestrial oxy-
411 gen reservoirs that are mass-dependently fractionated (*i.e.*, with $\Delta^{17}\text{O}$ of 0‰) (see Brenninkmeij-
412 er *et al.* (2003) and refs. therein). CO itself also has an unusual oxygen isotopic composition,
413 possessing a moderate tropospheric MIF of around +5‰ in $\Delta^{17}\text{O}(\text{CO})$ induced by the sink KIEs
414 in reaction of CO with OH (Röckmann *et al.*, 1998b; Röckmann *et al.*, 2002) and a minor
415 source effect from the ozonolysis of alkenes (Röckmann *et al.*, 1998a; Gromov *et al.*, 2010). A
416 substantial contamination of CO by O_3 oxygen induces proportional changes to $\Delta^{17}\text{O}(\text{CO})$ that
417 largely exceed its natural atmospheric variation. On the other hand, the MIF has implications in
418 the analytical determination of $\delta^{13}\text{C}(\text{CO})$, because the presence of C^{17}O species interferes with
419 the mass-spectrometric measurement of the abundances of ^{13}CO possessing the same basic mo-
420 lecular mass (m/z is 45). When inferring the exact $\text{C}^{17}\text{O}/\text{C}^{18}\text{O}$ ratio in the analysed sample is not
421 possible, analytical techniques usually involve assumptions (*e.g.*, mass-dependently fractionated

422 compositions or a certain non-zero $\Delta^{17}\text{O}$ value) with respect to the C^{17}O abundances
 423 (Assonov and Brenninkmeijer, 2001). In effect for the C1 CO data, the artefact CO produced
 424 from O_3 had contributed with unexpectedly high C^{17}O abundances that led to the overestimated
 425 $\delta^{13}\text{C}(\text{CO})$ analysed. The respective bias $^{13}\delta_b$ is quantified using

$$^{13}\delta_b = 7.26 \cdot 10^{-2} \Delta^{17}\text{O}(\text{CO}), \quad (\text{B1})$$

426 where the actual $\Delta^{17}\text{O}(\text{CO})$ value is approximated from the natural CO MIF signal $^{17}\Delta_n$ and the
 427 typical O_3 MIF composition $^{17}\Delta_c$ as

$$\Delta^{17}\text{O}(\text{CO}) = (^{17}\Delta_n([\text{CO}] - [\text{CO}_c]) + ^{17}\Delta_c[\text{CO}_c])([\text{CO}])^{-1}. \quad (\text{B2})$$

428 Here $[\text{CO}]$ and $[\text{CO}_c]$ denote the analysed CO mixing ratio and contamination magnitude, re-
 429 spectively, used in the contamination assessment (see Appendix A, Eq. (A4)) and in calcula-
 430 tions with the MM (see Sect. 3.1). For the purpose of the current estimate it is sufficient to take
 431 $^{17}\Delta_n$ of +5‰ representing equilibrium enrichments expected in the remote free troposphere and
 432 UT/LMS. For the O_3 MIF signature $^{17}\Delta_c$, the value of +30‰ (the average $\Delta^{17}\text{O}(\text{O}_3)$ expected
 433 from the kinetic laboratory data at conditions met along the C1 flight routes, see Sect. 3.2 and
 434 Table 1) is adopted. The coefficient that proportionates $^{13}\delta_b$ and $\Delta^{17}\text{O}$ in Eq. (B1) is derived by
 435 linearly regressing the $\delta^{13}\text{C}(\text{CO})$ biases (simulated using the calculation apparatus detailed by
 436 Assonov and Brenninkmeijer, 2001) as a function of $\Delta^{17}\text{O}(\text{CO})$ varying within a (0–30)‰
 437 range for the CO with initially unaccounted MIF (*e.g.*, the sample is assumed to be mass-
 438 dependently fractionated). It therefore quantifies some extra +(0.726±0.003)‰ in the analysed
 439 $\delta^{13}\text{C}(\text{CO})$ per every +10‰ of $\Delta^{17}\text{O}(\text{CO})$ excess. The most contaminated C1 WAS CO samples
 440 at $[\text{O}_3]$ above 300 nmol/mol are estimated to bear $\Delta^{17}\text{O}(\text{CO})$ of (6–12)‰ corresponding to frac-
 441 tions of (0.10–0.27) of the artefact CO in the sample. Accordingly, the reckoned $\delta^{13}\text{C}(\text{CO})$ bi-
 442 ases span (0.5–0.9)‰. Although not large, these well exceed the $\delta^{13}\text{C}(\text{CO})$ measurement preci-
 443 sion of ±0.1‰ and were corrected for, and therefore are taken into account in the calculations
 444 with the MM presented in Sect. 3.1.

445 **Acknowledgements**

446 [28] The authors are indebted to Claus Koepfel, Dieter Scharffe and Dr. Andreas Zahn for their
 447 work and expertise on the carbon monoxide and ozone measurements in C1 and C2. Hella
 448 Riede is acknowledged for comprehensive estimates of the species lifetimes along the
 449 CARIBIC flight routes. We are grateful to Dr. Taku Umezawa, Dr. Angela K. Baker, Dr. Em-

450 ma C. Leedham, Dr. Sergey Assonov, the anonymous reviewer and Dr. Jan Kaiser for the help-
451 ful discussions and comments on the manuscript.

452 **References**

- 453 Assonov, S. S. and Brenninkmeijer, C. A. M.: A new method to determine the ^{17}O isotopic abundance in
454 CO_2 using oxygen isotope exchange with a solid oxide, *Rapid Commun. Mass Spectrom.*, **15**,
455 2426–2437, doi: [10.1002/rcm.529](https://doi.org/10.1002/rcm.529), 2001.
- 456 Assonov, S. S. and Brenninkmeijer, C. A. M.: A redetermination of absolute values for $^{17}\text{R}_{\text{VPDB-CO}_2}$ and
457 $^{17}\text{R}_{\text{VSMOW}}$, *Rapid Commun. Mass Spectrom.*, **17**, 1017–1029, doi: [10.1002/Rcm.1011](https://doi.org/10.1002/Rcm.1011), 2003.
- 458 Assonov, S. S., Brenninkmeijer, C. A. M., Koepfel, C., and Röckmann, T.: CO_2 isotope analyses using
459 large air samples collected on intercontinental flights by the CARIBIC Boeing 767,
460 *Rapid Commun. Mass Spectrom.*, **23**, 822–830, doi: [10.1002/rcm.3946](https://doi.org/10.1002/rcm.3946), 2009.
- 461 Bhattacharya, S. K., Pandey, A., and Savarino, J.: Determination of intramolecular isotope distribution of
462 ozone by oxidation reaction with silver metal, *J. Geophys. Res. Atm.*, **113**, D033303,
463 doi: [10.1029/2006jd008309](https://doi.org/10.1029/2006jd008309), 2008.
- 464 Brenninkmeijer, C. A. M.: Measurement of the abundance of ^{14}CO in the atmosphere and the $^{13}\text{C}/^{12}\text{C}$ and
465 $^{18}\text{O}/^{16}\text{O}$ ratio of atmospheric CO with applications in New Zealand and
466 Antarctica, *J. Geophys. Res. Atm.*, **98**, 10595–10614, doi: [10.1029/93JD00587](https://doi.org/10.1029/93JD00587), 1993.
- 467 Brenninkmeijer, C. A. M., Müller, R., Crutzen, P. J., Lowe, D. C., Manning, M. R., Sparks, R. J., and van
468 Velthoven, P. F. J.: A large ^{13}C deficit in the lower Antarctic stratosphere due to “Ozone Hole”
469 Chemistry: Part I, Observations, *Geophys. Res. Lett.*, **23**, 2125–2128, doi: [10.1029/96gl01471](https://doi.org/10.1029/96gl01471), 1996.
- 470 Brenninkmeijer, C. A. M. and Röckmann, T.: Principal factors determining the $^{18}\text{O}/^{16}\text{O}$ ratio of
471 atmospheric CO as derived from observations in the southern hemispheric troposphere and lowermost
472 stratosphere, *J. Geophys. Res. Atm.*, **102**, 25477–25485, doi: [10.1029/97JD02291](https://doi.org/10.1029/97JD02291), 1997.
- 473 Brenninkmeijer, C. A. M., Crutzen, P. J., Fischer, H., Gusten, H., Hans, W., Heinrich, G.,
474 Heintzenberg, J., Hermann, M., Immelmann, T., Kersting, D., Maiss, M., Nolle, M., Pitscheider, A.,
475 Pohlkamp, H., Scharffe, D., Specht, K., and Wiedensohler, A.: CARIBIC – Civil aircraft for global
476 measurement of trace gases and aerosols in the tropopause region, *J. Atmos. Oceanic Technol.*, **16**,
477 1373–1383, doi: [10.1175/1520-0426\(1999\)016<1373:Ccafgm>2.0.Co;2](https://doi.org/10.1175/1520-0426(1999)016<1373:Ccafgm>2.0.Co;2), 1999.
- 478 Brenninkmeijer, C. A. M., Koepfel, C., Röckmann, T., Scharffe, D. S., Bränlich, M., and Gros, V.:
479 Absolute measurement of the abundance of atmospheric carbon monoxide, *J. Geophys. Res. Atm.*, **106**,
480 10003–10010, doi: [10.1029/2000jd900342](https://doi.org/10.1029/2000jd900342), 2001.
- 481 Brenninkmeijer, C. A. M., Janssen, C., Kaiser, J., Röckmann, T., Rhee, T. S., and Assonov, S. S.: Isotope
482 effects in the chemistry of atmospheric trace compounds, *Chem. Rev.*, **103**, 5125–5161,
483 doi: [10.1021/Cr020644k](https://doi.org/10.1021/Cr020644k), 2003.
- 484 Brenninkmeijer, C. A. M., Crutzen, P., Boumard, F., Dauer, T., Dix, B., Ebinghaus, R., Filippi, D.,
485 Fischer, H., Franke, H., Frieß, U., Heintzenberg, J., Helleis, F., Hermann, M., Kock, H. H.,
486 Koepfel, C., Lelieveld, J., Leuenberger, M., Martinsson, B. G., Miemczyk, S., Moret, H. P.,
487 Nguyen, H. N., Nyfeler, P., Oram, D., O'Sullivan, D., Penkett, S., Platt, U., Pupek, M., Ramonet, M.,
488 Randa, B., Reichelt, M., Rhee, T. S., Rohwer, J., Rosenfeld, K., Scharffe, D., Schlager, H.,
489 Schumann, U., Slemr, F., Sprung, D., Stock, P., Thaler, R., Valentino, F., van Velthoven, P.,

490 Waibel, A., Wandel, A., Waschitschek, K., Wiedensohler, A., Xueref-Remy, I., Zahn, A.,
 491 Zech, U., and Ziereis, H.: Civil Aircraft for the regular investigation of the atmosphere based on an
 492 instrumented container: The new CARIBIC system, *Atmos. Chem. Phys.*, **7**, 4953–4976,
 493 doi: [10.5194/acp-7-4953-2007](https://doi.org/10.5194/acp-7-4953-2007), 2007.

494 Coplen, T. B.: Reporting of stable hydrogen, carbon, and oxygen isotopic abundances (Technical Report),
 495 *Pure Appl. Chem.*, **66**, 273–276, doi: [10.1351/pac199466020273](https://doi.org/10.1351/pac199466020273), 1994.

496 Craig, H.: Isotopic standards for carbon and oxygen and correction factors for mass-spectrometric analysis
 497 of carbon dioxide, *Geochim. Cosmochim. Acta*, **12**, 133–149, doi: [10.1016/0016-7037\(57\)90024-8](https://doi.org/10.1016/0016-7037(57)90024-8),
 498 1957.

499 Gonfiantini, R.: Standards for Stable Isotope Measurements in Natural Compounds, *Nature*, **271**,
 500 534–536, 1978.

501 Gromov, S., Jöckel, P., Sander, R., and Brenninkmeijer, C. A. M.: A kinetic chemistry tagging technique
 502 and its application to modelling the stable isotopic composition of atmospheric trace gases,
 503 *Geosci. Model Dev.*, **3**, 337–364, doi: [10.5194/gmd-3-337-2010](https://doi.org/10.5194/gmd-3-337-2010), 2010.

504 Guenther, J., Erbacher, B., Krankowsky, D., and Mauersberger, K.: Pressure dependence of two relative
 505 ozone formation rate coefficients, *Chem. Phys. Lett.*, **306**, 209–213,
 506 doi: [10.1016/S0009-2614\(99\)00469-8](https://doi.org/10.1016/S0009-2614(99)00469-8), 1999.

507 Janssen, C., Guenther, J., Krankowsky, D., and Mauersberger, K.: Temperature dependence of ozone rate
 508 coefficients and isotopologue fractionation in ^{16}O – ^{18}O oxygen mixtures, *Chem. Phys. Lett.*, **367**,
 509 34–38, doi: [10.1016/S0009-2614\(02\)01665-2](https://doi.org/10.1016/S0009-2614(02)01665-2), 2003.

510 Janssen, C.: Intramolecular isotope distribution in heavy ozone ($^{16}\text{O}^{18}\text{O}^{16}\text{O}$ and $^{16}\text{O}^{16}\text{O}^{18}\text{O}$),
 511 *J. Geophys. Res. Atm.*, **110**, D08308, doi: [10.1029/2004jd005479](https://doi.org/10.1029/2004jd005479), 2005.

512 Johnston, J. C. and Thieme, M. H.: The isotopic composition of tropospheric ozone in three
 513 environments, *J. Geophys. Res. Atm.*, **102**, 25395–25404, doi: [10.1029/97jd02075](https://doi.org/10.1029/97jd02075), 1997.

514 Krankowsky, D., Bartecki, F., Klees, G. G., Mauersberger, K., Schellenbach, K., and Stehr, J.:
 515 Measurement of heavy isotope enrichment in tropospheric ozone, *Geophys. Res. Lett.*, **22**, 1713–1716,
 516 doi: [10.1029/95gl01436](https://doi.org/10.1029/95gl01436), 1995.

517 Krankowsky, D., Lämmerzahl, P., Mauersberger, K., Janssen, C., Tuzson, B., and Röckmann, T.:
 518 Stratospheric ozone isotope fractionations derived from collected samples, *J. Geophys. Res. Atm.*, **112**,
 519 D08301, doi: [10.1029/2006jd007855](https://doi.org/10.1029/2006jd007855), 2007.

520 Li, W., Gibbs, G. V., and Oyama, S. T.: Mechanism of Ozone Decomposition on a Manganese Oxide
 521 Catalyst. 1. In Situ Raman Spectroscopy and Ab Initio Molecular Orbital
 522 Calculations, *J. Am. Chem. Soc.*, **120**, 9041–9046, doi: [10.1021/ja981441+](https://doi.org/10.1021/ja981441+), 1998.

523 Mauersberger, K.: Measurement of Heavy Ozone in the Stratosphere, *Geophys. Res. Lett.*, **8**, 935–937,
 524 doi: [10.1029/GI008i008p00935](https://doi.org/10.1029/GI008i008p00935), 1981.

525 McNaught, A. D. and Wilkinson, A.: IUPAC. Compendium of Chemical Terminology (the "Gold Book"),
 526 XML on-line corrected version: <http://goldbook.iupac.org> (2006-) created by
 527 M. Nic, J. Jirat, B. Kosata; updates compiled by A. Jenkins, doi: [10.1351/goldbook.O04322](https://doi.org/10.1351/goldbook.O04322), 1997.

528 Natrella, M.: NIST/SEMATECH e-Handbook of Statistical Methods, edited by: Croarkin, C. and
 529 Tobias, P., NIST/SEMATECH, <http://www.itl.nist.gov/div898/handbook/> (last access: 07 May 2014),
 530 2003.

531 Novelli, P. C., Masarie, K. A., and Lang, P. M.: Distributions and recent changes of carbon monoxide in
 532 the lower troposphere, *J. Geophys. Res.*, **103**, 19015–19033, doi: [10.1029/98jd01366](https://doi.org/10.1029/98jd01366), 1998.

- 533 Novelli, P. C., Masarie, K. A., Lang, P. M., Hall, B. D., Myers, R. C., and Elkins, J. W.: Reanalysis of
534 tropospheric CO trends: Effects of the 1997–1998 wildfires, *J. Geophys. Res.*, **108**, 4464,
535 doi: [10.1029/2002jd003031](https://doi.org/10.1029/2002jd003031), 2003.
- 536 Oyama, S. T.: Chemical and Catalytic Properties of Ozone, *Catal. Rev. Sci. Eng.*, **42**, 279–322,
537 doi: [10.1081/cr-100100263](https://doi.org/10.1081/cr-100100263), 2000.
- 538 Pan, L. L., Randel, W. J., Gary, B. L., Mahoney, M. J., and Hints, E. J.: Definitions and sharpness of the
539 extratropical tropopause: A trace gas perspective, *J. Geophys. Res. Atm.*, **109**, D23103,
540 doi: [10.1029/2004jd004982](https://doi.org/10.1029/2004jd004982), 2004.
- 541 Röckmann, T., Brenninkmeijer, C. A. M., Neeb, P., and Crutzen, P. J.: Ozonolysis of nonmethane
542 hydrocarbons as a source of the observed mass independent oxygen isotope enrichment in tropospheric
543 CO, *J. Geophys. Res. Atm.*, **103**, 1463–1470, doi: [10.1029/97JD02929](https://doi.org/10.1029/97JD02929), 1998a.
- 544 Röckmann, T., Brenninkmeijer, C. A. M., Saueressig, G., Bergamaschi, P., Crowley, J. N.,
545 Fischer, H., and Crutzen, P. J.: Mass-independent oxygen isotope fractionation in atmospheric CO as a
546 result of the reaction CO+OH, *Science*, **281**, 544–546, doi: [10.1126/science.281.5376.544](https://doi.org/10.1126/science.281.5376.544), 1998b.
- 547 Röckmann, T., Jöckel, P., Gros, V., Bräunlich, M., Possnert, G., and Brenninkmeijer, C. A. M.: Using ¹⁴C,
548 ¹³C, ¹⁸O and ¹⁷O isotopic variations to provide insights into the high northern latitude surface CO
549 inventory, *Atmos. Chem. Phys.*, **2**, 147–159, doi: [10.5194/acp-2-147-2002](https://doi.org/10.5194/acp-2-147-2002), 2002.
- 550 Savarino, J., Bhattacharya, S. K., Morin, S., Baroni, M., and Doussin, J. F.: The NO+O₃ reaction: A triple
551 oxygen isotope perspective on the reaction dynamics and atmospheric implications for the transfer of
552 the ozone isotope anomaly, *J. Chem. Phys.*, **128**, 194303, doi: [10.1063/1.2917581](https://doi.org/10.1063/1.2917581), 2008.
- 553 Savarino, J. and Morin, S.: The N, O, S Isotopes of Oxy-Anions in Ice Cores and Polar Environments, in:
554 Handbook of Environmental Isotope Geochemistry, edited by: Baskaran, M., Advances in Isotope
555 Geochemistry, Springer Berlin Heidelberg, 835–864, 2012.
- 556 Scharffe, D., Slemr, F., Brenninkmeijer, C. A. M., and Zahn, A.: Carbon monoxide measurements onboard
557 the CARIBIC passenger aircraft using UV resonance fluorescence, *Atmos. Meas. Tech.*, **5**, 1753–1760,
558 doi: [10.5194/amt-5-1753-2012](https://doi.org/10.5194/amt-5-1753-2012), 2012.
- 559 Schinke, R., Grebenshchikov, S. Y., Ivanov, M. V., and Fleurat-Lessard, P.: Dynamical Studies Of The
560 Ozone Isotope Effect: A Status Report, *Annu. Rev. Phys. Chem.*, **57**, 625–661,
561 doi: [10.1146/annurev.physchem.57.032905.104542](https://doi.org/10.1146/annurev.physchem.57.032905.104542), 2006.
- 562 Stevens, C. M., Kaplan, L., Gorse, R., Durkee, S., Compton, M., Cohen, S., and Bielling, K.: The Kinetic
563 Isotope Effect for Carbon and Oxygen in the Reaction CO+OH, *Int. J. Chem. Kinet.*, **12**, 935–948,
564 doi: [10.1002/kin.550121205](https://doi.org/10.1002/kin.550121205), 1980.
- 565 Vicars, W. C., Bhattacharya, S. K., Erbland, J., and Savarino, J.: Measurement of the ¹⁷O-excess ($\Delta^{17}\text{O}$) of
566 tropospheric ozone using a nitrite-coated filter, *Rapid Commun. Mass Spectrom.*, **26**, 1219–1231,
567 doi: [10.1002/rcm.6218](https://doi.org/10.1002/rcm.6218), 2012.
- 568 Vicars, W. C. and Savarino, J.: Quantitative constraints on the ¹⁷O-excess ($\Delta^{17}\text{O}$) signature of surface
569 ozone: Ambient measurements from 50°N to 50°S using the nitrite-coated filter technique,
570 *Geochim. Cosmochim. Acta*, **135**, 270–287, doi: [10.1016/j.gca.2014.03.023](https://doi.org/10.1016/j.gca.2014.03.023), 2014.
- 571 Zahn, A., Brenninkmeijer, C. A. M., Maiss, M., Scharffe, D. H., Crutzen, P. J., Hermann, M.,
572 Heintzenberg, J., Wiedensohler, A., Güsten, H., Heinrich, G., Fischer, H., Cuijpers, J. W. M., and van
573 Velthoven, P. F. J.: Identification of extratropical two-way troposphere-stratosphere mixing based on
574 CARIBIC measurements of O₃, CO, and ultrafine particles, *J. Geophys. Res.*, **105**, 1527–1535,
575 doi: [10.1029/1999jd900759](https://doi.org/10.1029/1999jd900759), 2000.

576 Zahn, A., Brenninkmeijer, C. A. M., Asman, W. A. H., Crutzen, P. J., Heinrich, G., Fischer, H.,
577 Cuijpers, J. W. M., and van Velthoven, P. F. J.: Budgets of O₃ and CO in the upper troposphere:
578 CARIBIC passenger aircraft results 1997–2001, *J. Geophys. Res. Atm.*, **107**, 4337,
579 doi: [10.1029/2001jd001529](https://doi.org/10.1029/2001jd001529), 2002.

580 Zahn, A., Weppner, J., Widmann, H., Schlote-Holubek, K., Burger, B., Kühner, T., and Franke, H.: A fast
581 and precise chemiluminescence ozone detector for eddy flux and airborne application,
582 *Atmos. Meas. Tech.*, **5**, 363–375, doi: [10.5194/amt-5-363-2012](https://doi.org/10.5194/amt-5-363-2012), 2012.

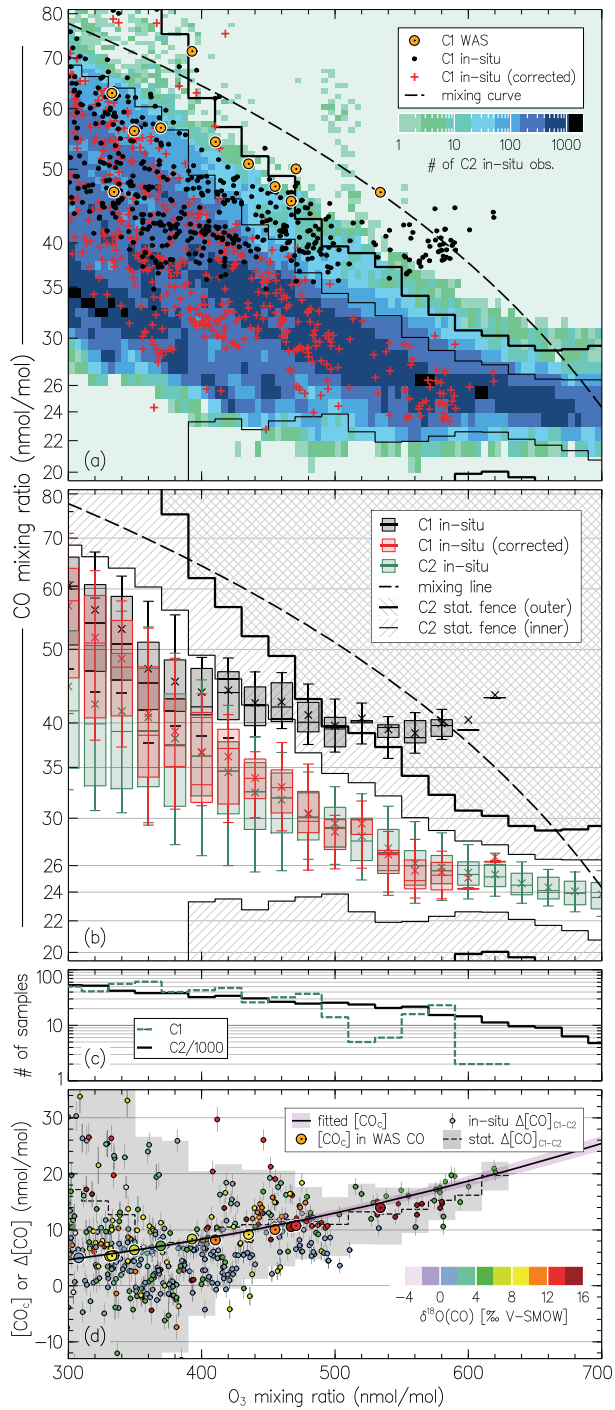
583 Tables

584 Table 1. Ozone ¹⁸O/¹⁶O isotope ratios from literature and this study

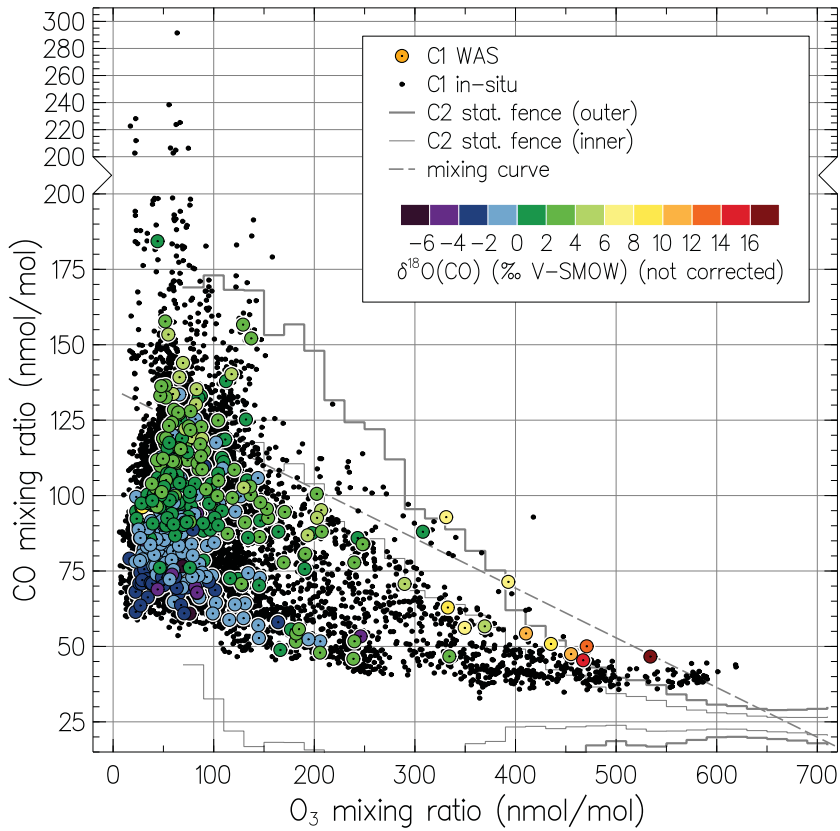
Domain	T (K)	P (hPa)	δ ¹⁸ O(O ₃) (‰)	Remarks
Stratosphere	190–210	13–50	83–93 (<3)	1
UT/LMS	220–235	240–270	89–95 (8)	2
			84–88 (6)	T
			91–98 (9)	TC
			112–124 (17)	C
Laboratory	190–210	67	87–97 (6)	3
	220–235	67	102–110 (6)	3
	220–235	240–270	95–103	4

Notes: Values in parentheses denote the average of the estimates' standard errors. The expected O₃ isotope composition on the VSMOW scale is calculated from the O₃ enrichments reported relative to O₂ using $\delta^{18}\text{O}(\text{O}_3)_{\text{VSMOW}} = \delta^{18}\text{O}(\text{O}_2)_{\text{VSMOW}} + {}^{18}\delta(\text{O}_3)_{\text{Air-O}_2} + [\delta^{18}\text{O}(\text{O}_2)_{\text{VSMOW}} \times {}^{18}\epsilon(\text{O}_3)_{\text{Air-O}_2}]$.

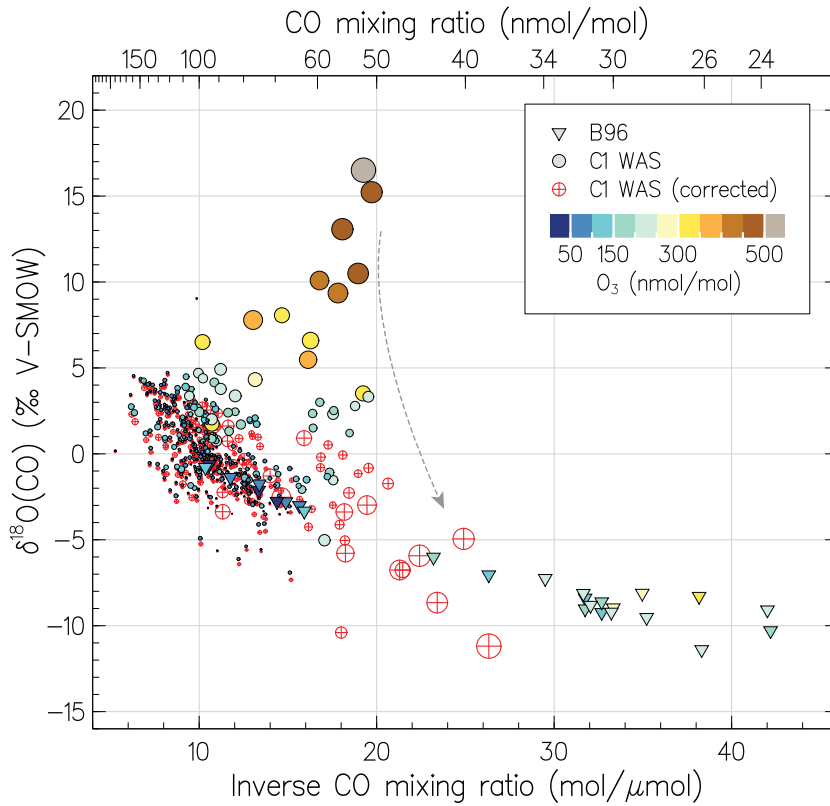
- ¹ Observations (see Krankowsky *et al.* (2007) and refs. therein), lowermost values (19–25 km). Quoted temperature range is derived by matching measured δ¹⁸O(O₃) and laboratory data (see note ³).
- ² This study, C1 observations (10–12 km). Letters denote the estimates derived using the data from Bhattacharya *et al.* (2008) and assuming only terminal (T), only central (C) and equiprobable terminal and central (TC) O₃ atoms transfer to the artefact CO.
- ³ Calculated using the laboratory KIE temperature dependence data summarised by Janssen *et al.* (2003).
- ⁴ Calculated assuming a pressure dependence of the O₃ formation KIE similar to that measured at 320 K (see Guenther *et al.* (1999) and refs. therein).



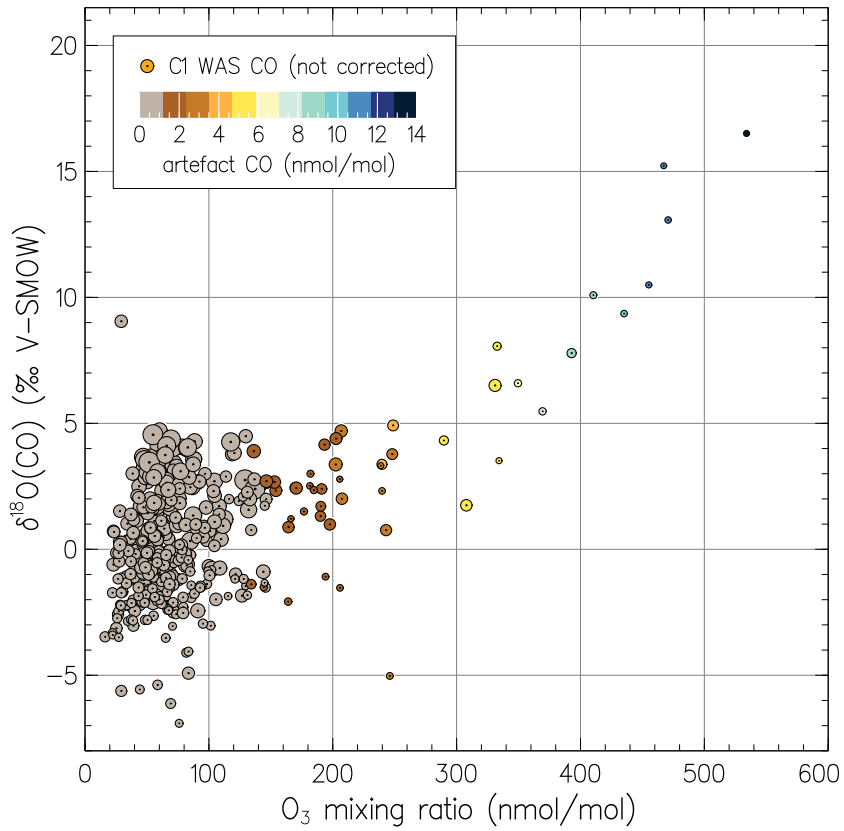
586 Fig. 1. (a) Distribution of CO mixing ratios as a function of concomitant O₃ mixing ratios measured by
587 CARIBIC in the LMS ([O₃] > 300 nmol/mol). The shaded area is the two-dimensional histogram of the C2
588 measurements (all C2 data obtained until June 2013) counted in 5 × 1 nmol/mol size [O₃] × [CO] bins, thus
589 darker areas emphasise greater numbers of particular CO–O₃ pairs observed. Small symbols denote the
590 original C1 *in situ* measurements (black) and corrected for the artefacts (red); the C1 WAS analyses (11 of
591 total 408) are shown with large symbols. Thin and thick step-lines demark the inner and outer statistical
592 fences (ranges outside which the data points are considered mild or extreme outliers, see text) of the C2
593 data, respectively. The dashed curve exemplifies compositions expected from the linear mixing of very
594 different (*e.g.*, tropospheric and stratospheric) end-members. (b) Statistics on CO mixing ratios from C1
595 and C2 data shown in box-and-whisker diagrams for samples clustered in 20 nmol/mol O₃ bins (whiskers
596 represent 9th/91st percentiles). (c) Sample statistic for each CARIBIC dataset (note the C2 figures scaled
597 down by a factor of 1000). (d) Estimates of the C1 *in situ* CO contamination strength [CO_c] as a function
598 of [O₃] (solid line) obtained by fitting the difference Δ[CO] between the C2 and C1 *in situ* [CO] (small
599 symbols) as detailed in Appendix A (Eq. (A2)). Step line shows the Δ[CO] for the statistical averages (the
600 shaded area equals the height of the inner statistical fences of the C2 data). Large symbols denote the es-
601 timates of [CO_c] in the C1 WAS data (slight variations *vs.* the *in situ* data are due to the sample mixing ef-
602 fects, see Sect. 3). Colour denotes the respective C1 WAS δ¹⁸O(CO) (note that typically 6–7 *in situ* meas-
603 urements correspond to one WAS sample).



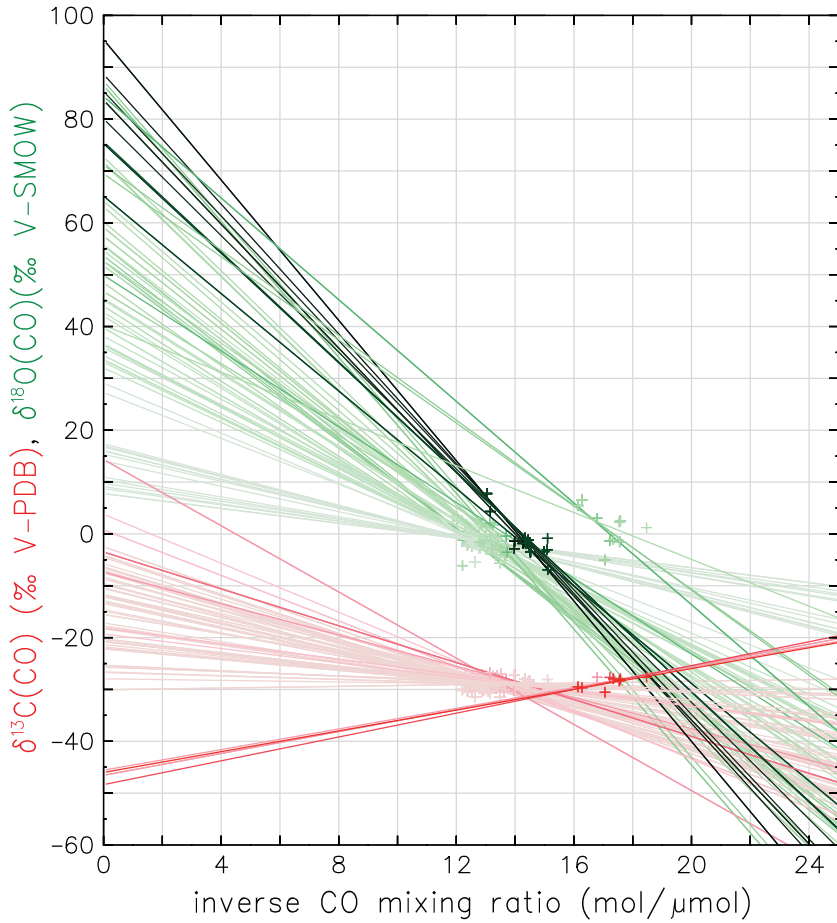
604 Fig. 2. (accompanies Fig. 1) Carbon monoxide and ozone mixing ratios measured in C1. Small black sym-
 605 bols denote the C1 *in situ* measurements ($n = 12753$). The C1 WAS analyses ($n = 408$) are shown with
 606 large symbols; colour denotes the concomitant $\delta^{18}\text{O}(\text{CO})$ measurements. Thin and thick step-lines denote
 607 the inner and outer statistical fences of the C2 data, respectively. The dashed curve exemplifies composi-
 608 tions expected from the linear mixing of tropospheric and stratospheric end-members (see caption to Fig. 1
 609 for details).



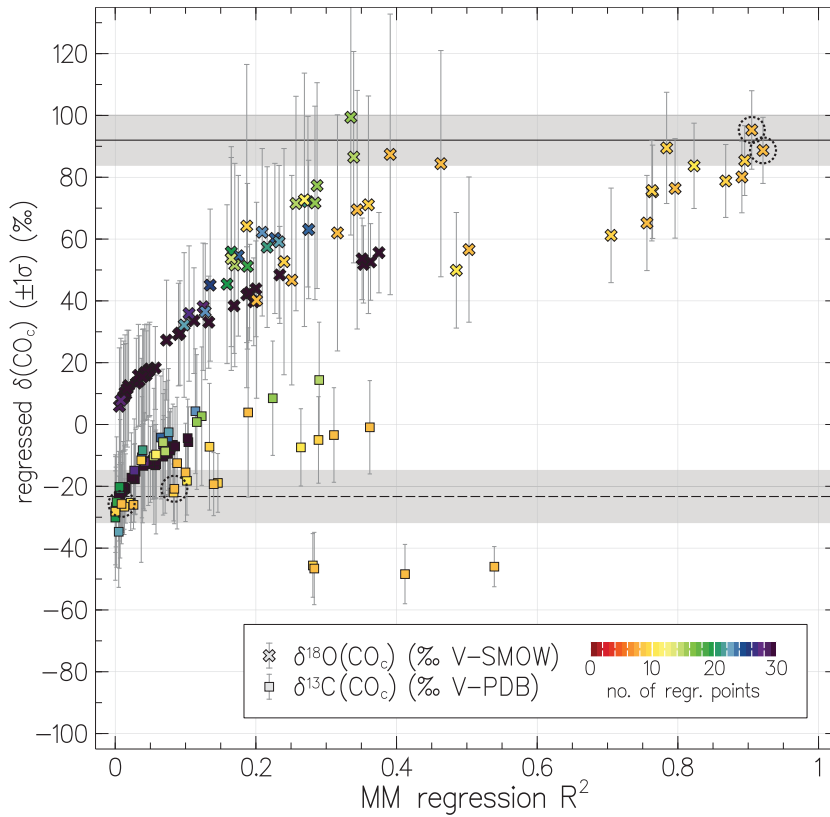
610 Fig. 3. $^{18}\text{O}/^{16}\text{O}$ isotope composition of CO as a function of its reciprocal mixing ratio. Triangles present
 611 the data from the remote SH UT/LMS obtained by Brenninkmeijer *et al.* (1996) (B96). Colour refers to the
 612 concomitantly observed O_3 abundances; note the extremely low $[\text{O}_3]$ encountered by B96 in the Antarctic
 613 "ozone hole" conditions. Filled and hollow circles denote the original and corrected (as exemplified by the
 614 dashed arrow) C1 WAS data, respectively, with the symbol size scaling proportional to the estimated con-
 615 tamination magnitude (see text).



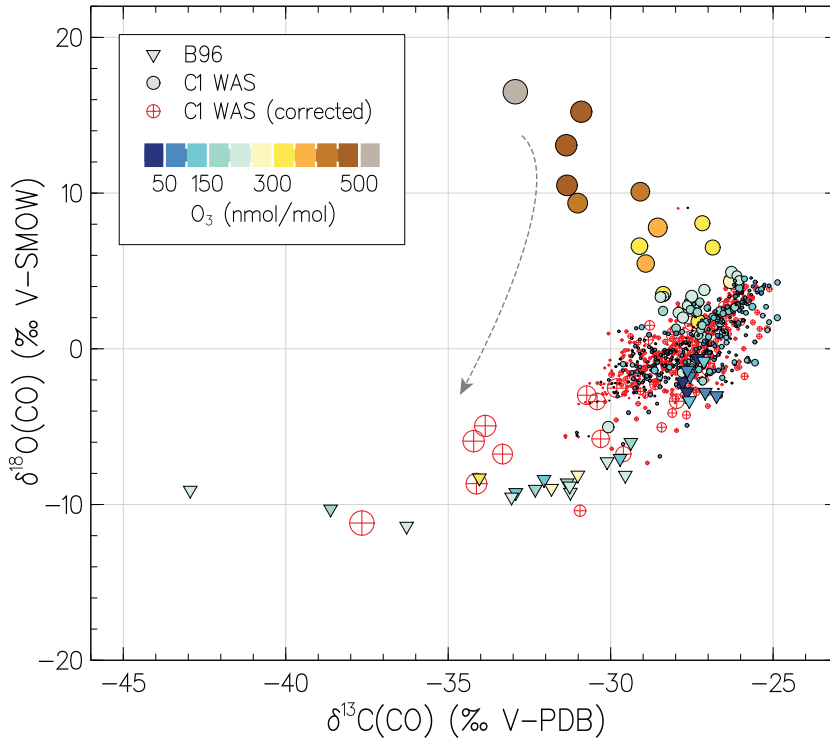
616 Fig. 4. Measured C1 WAS $\delta^{18}\text{O}(\text{CO})$ (not corrected for artefacts) as a function of concomitant O_3 mixing
 617 ratio. Symbol colour denotes the artefact CO component (integral $[\text{CO}_c]$ per each WAS); symbol size
 618 scales proportionally to the WAS CO mixing ratio corrected for artefacts (see Sect. 3 for details).



619 Fig. 5. Keeling plot of the data used in the calculations with the mixing model (MM). The C1 WAS iso-
 620 tope CO measurements are shown with symbols, solid lines denote the linear regressions through the vari-
 621 ous sets of samples selected by the MM ($n = 80$ sets are plotted). Colours refer to the $\delta^{13}\text{C}$ (red) and $\delta^{18}\text{O}$
 622 (green) data, colour intensity indicates the coefficient of determination (R^2) of each regression, respective-
 623 ly. Darker colours denote higher R^2 values, with maxima of 0.92 for $\delta^{18}\text{O}$ and 0.54 for $\delta^{13}\text{C}$ data, respec-
 624 tively. The inferred contamination signatures $\delta(\text{CO}_c)$ are found at $([\text{CO}])^{-1} \rightarrow 0$. Regression uncertainties
 625 are shown in Fig. 6. Note that because different subsets of samples contain same data points, some of the
 626 symbols are plotted over (*i.e.*, not all symbols contributing to a particular regression case may be seen).



627 Fig. 6. Results of the regression calculation with the MM. Shown with symbols are the contamination
 628 source isotope signatures $\delta(\text{CO}_c)$ as a function of the respective coefficient of determination (R^2). Colour
 629 denotes the number of samples in each subset selected. Solid and dashed lines present the best guess
 630 ± 1 standard deviation of the mean for the $\delta^{18}\text{O}(\text{CO}_c)$ and $\delta^{13}\text{C}(\text{CO}_c)$ estimates. Dashed circles mark the es-
 631 timates obtained at highest R^2 for $\delta^{18}\text{O}(\text{CO}_c)$ regression (above 0.9). See text for details.



632 Fig. 7. $^{18}\text{O}/^{16}\text{O}$ and $^{13}\text{C}/^{12}\text{C}$ isotope composition of CO measured in C1. Triangles present the data from the
 633 remote SH UT/LMS obtained by Brenninkmeijer *et al.* (1996) (B96). Colour refers to the concomitantly
 634 observed O_3 abundances; note the extremely low $[\text{O}_3]$ encountered by B96 in the Antarctic ozone-hole
 635 conditions. Filled and hollow circles denote the original and corrected (as exemplified by the dashed ar-
 636 row) C1 WAS data, respectively, with the symbol size scaling proportional to the estimated contamination
 637 magnitude (see text for details).